

Pathway Switching Explains the Sharp Response Characteristic of Hypoxia Response Network

Yihai Yu¹, Guanyu Wang¹, Rahul Simha², Weiqun Peng¹, Frank Turano³, Chen Zeng^{1*}

1 Department of Physics, George Washington University, Washington, D.C., United States of America, **2** Department of Computer Sciences, George Washington University, Washington, D.C., United States of America, **3** Department of Biological Sciences, George Washington University, Washington, D.C., United States of America

Hypoxia induces the expression of genes that alter metabolism through the hypoxia-inducible factor (HIF). A theoretical model based on differential equations of the hypoxia response network has been previously proposed in which a sharp response to changes in oxygen concentration was observed but not quantitatively explained. That model consisted of reactions involving 23 molecular species among which the concentrations of HIF and oxygen were linked through a complex set of reactions. In this paper, we analyze this previous model using a combination of mathematical tools to draw out the key components of the network and explain quantitatively how they contribute to the sharp oxygen response. We find that the switch-like behavior is due to pathway-switching wherein HIF degrades rapidly under normoxia in one pathway, while the other pathway accumulates HIF to trigger downstream genes under hypoxia. The analytic technique is potentially useful in studying larger biomedical networks.

Citation: Yu Y, Wang G, Simha R, Peng W, Turano F, et al. (2007) Pathway switching explains the sharp response characteristic of hypoxia response network. *PLoS Comput Biol* 3(8): e171. doi:10.1371/journal.pcbi.0030171

Introduction

Molecular oxygen is the terminal electron acceptor in the mitochondrial electron transport chain. Hypoxia, or oxygen deficiency, induces a number of metabolic changes with rapid and profound consequences on cell physiology. A hypoxia-induced shortage of energy alters gene expression, energy consumption, and cellular metabolism to allow for continued energy generation despite diminished oxygen availability. A molecular interaction map of the hypoxia response network has been proposed [1–3] on the basis of analyzing conserved components between nematodes and mammals. The key element in this network, hypoxia-inducible factor (HIF), is a master regulator of oxygen-sensitive gene expression [4–6]. HIF is a heterodimeric transcription factor which consists of one of the three different members (HIF-1 α , HIF-2 α , and HIF-3 α) and a common constitutive ARNT subunit which is also known as HIF β . The system also includes an enzyme family: prolyl hydroxylases (PHDs), which directly sense the level of oxygen and hydroxylate HIF α by covalently modifying the HIF α subunits. It is very likely that reactive oxidative species (ROS), which are a byproduct of mitochondrial respiration, are also involved in oxygen sensing by neutralizing a necessary cofactor, Fe²⁺, for the hydroxylation of HIF α by a PHD [7–10]. There are three members in this enzyme family: PHD1, PHD2, and PHD3. The hydroxylated HIF α is then targeted by the von Hippel-Lindau tumor-suppressor protein (VHL) for the ubiquitination-dependent degradation. Hypoxia response element (HRE) is the promoter of the hypoxia-regulated genes, and the occupancy of HRE controls the expression levels of these genes. The cascade in Figure 1 (reproduced from Figure 2 of [1]) consists of an input (the concentration of oxygen) and an output (the activation of promoters that are under control of HREs) as the core network. The network is characterized by a switch-like behavior, namely the sharp increase of HIF α when the oxygen decreases below a critical value, followed by a sharp increase of HRE occupancy. It was observed experimentally

on many cell lines including HeLa cells [11] and Hep 3B cells [12] that HIF α increases exponentially as the oxygen concentration decreases.

The past two decades have seen a growing body of work on the use of mathematical modeling to help uncover both general principles behind molecular networks and to provide quantitative explanations of particular network phenomena [13] that may one day have sufficient predictive power to accurately model large subnetworks of the cell. In this sense, Kohn et al. [1] have successfully modeled the switch-like response characteristics of HRE occupancy, by numerically integrating a system of ordinary differential equations (ODEs) involving a score of molecular species related to hypoxia. The large model, however, does not identify the smaller components that are actually responsible for the switch-like response and that may occur in other such networks. Furthermore, a numerical solution does not provide the type of insight that mathematical formulas can. At the same time, it is virtually impossible to solve symbolically the type of nonlinear differential equations that model reactions. In this context, methods are desirable that are both tractable, that reduce a system to its key components, and that are not solely reliant on numerical solution.

Extreme pathway analysis (EPA) is one such recently

Editor: Adam P. Arkin, Lawrence Berkeley National Laboratory, United States of America

Received: February 8, 2007; **Accepted:** July 19, 2007; **Published:** August 31, 2007

A previous version of this article appeared as an Early Online Release on July 20, 2007 (doi:10.1371/journal.pcbi.0030171.eor).

Copyright: © 2007 Yu et al. This is an open-access article distributed under the terms of the Creative Commons Attribution License, which permits unrestricted use, distribution, and reproduction in any medium, provided the original author and source are credited.

Abbreviations: EPA, extreme pathway analysis; HIF, hypoxia-inducible factor; HRE, hypoxia response element; PHD, prolyl hydroxylase; ROS, reactive oxidative species; VHL, von Hippel-Lindau tumor-suppressor protein

* To whom correspondence should be addressed. E-mail: chenz@gwu.edu

Author Summary

A complex biomolecular network utilizes different pathways to perform different functions. However, the interactions within the network are typically so complicated that the pathway structure is usually hidden. By some mathematical techniques, the pathways can be identified and possibly decoupled, whereby the insightful details of the network can be exposed. As an example, we study in this paper the hypoxia response network that manifests a dramatic switch-like behavior for certain sets of rate constants: a slight change of the oxygen concentration close to a critical value will lead to distinct reaction patterns. By a technique called extreme pathway analysis, the network is decoupled into three major and some minor pathways. Flux distribution among these pathways can thus be measured by integrating the ordinary differential equations for any given set of rate constants. For the sets of rate constants where the switch-like behavior is observed, we found that such a behavior is due to the switching of flux between two of the three major pathways.

developed method [14–16]. In this method, the dynamics of interactions between species are formulated as a Boolean network in which the state of a gene is represented as either transcribed or not transcribed. Upregulation and downregulation of genes are captured through an appropriate sign (plus or minus) and a scaling constant. The Boolean network is then formulated as a matrix of interaction rules that is then analyzed to help reveal key components and their contributions to the dynamic behavior [16]. The theory of matrices then allows us to look for vectors that characterize the matrix in ways that are helpful for further analysis. The EPA technique, in particular, finds vectors (extreme pathways) that correspond to the boundaries of the space of steady-state

solutions to the differential equations. We note that similar methods, such as flux balance analysis (FBA) and elementary modes analysis, have been developed in other contexts [17–19]. They essentially yield the same results [18], which have been verified by ExPa [20] and CellNetAnalyzer [21,22]. These methods provide a way out of the intractable complexity of sizable molecular networks [23–26].

Our contribution is to go beyond this type of matrix approach and provide a detailed quantitative analysis that explains the observed behavior in the models. This is achieved by combining elementary pathway identification via EPA, which depends solely on the network topology, and the detailed analytical as well as numerical analysis of the governing differential equations in the model, which allows studies of the phase space spanned by the mostly unknown rate constants in the differential equations. Specifically, EPA is first used in our approach to decompose the original network into several underlying pathways. Following this, we make some reasonable approximations to facilitate analytic solution. We show that this analytic solution, in the case of the hypoxia network, explains the switch-like behavior. This explanation is confirmed by comparing the numerical output of the simplified model with the numerical output of the complete (and complex) differential equation model.

A second contribution of this paper is to highlight a particular mechanism of pathway-switching or pathway branching effect [27] that appears to cause the sharp response to oxygen concentration. In particular, we examine the flux redistribution among the elementary pathways as a function of oxygen concentration. We also identify the key molecular species involved in the subcomponent of the network and show quantitatively how the response of this subcomponent

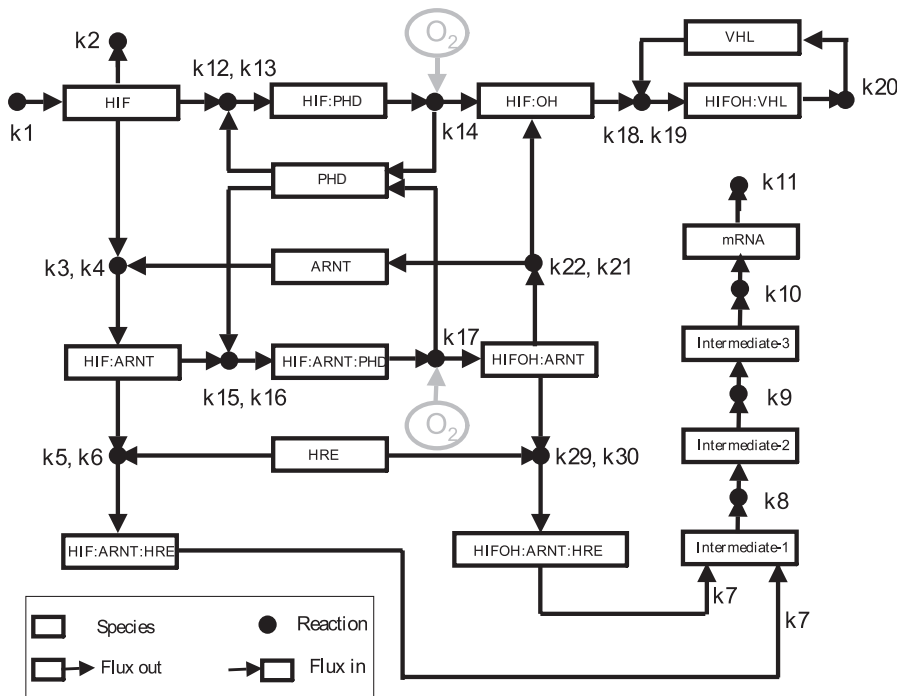


Figure 1. Diagram of the Assumed Core Subsystem of the Hypoxia Response Network Redrawn on the Basis of [1] For simplicity we use HIF to represent HIF α .
doi:10.1371/journal.pcbi.0030171.g001

	k_1	k_2	k_3	k_4	k_5	k_6	k_{12}	k_{13}	k_{14}	k_{15}	k_{16}	k_{17}	k_{18}	k_{19}	k_{20}	k_{21}	k_{22}	k_{29}	k_{30}		
$\Phi =$	1	-1	-1	1	0	0	-1	1	0	0	0	0	0	0	0	0	0	0	0	0	S_3
	0	0	-1	1	0	0	0	0	0	0	0	0	0	0	0	0	-1	1	0	0	S_4
	0	0	1	-1	-1	1	0	0	0	-1	1	0	0	0	0	0	0	0	0	0	S_5
	0	0	0	0	-1	1	0	0	0	0	0	0	0	0	0	0	0	0	-1	1	S_6
	0	0	0	0	1	-1	0	0	0	0	0	0	0	0	0	0	0	0	0	0	S_7
	0	0	0	0	0	0	-1	1	1	-1	1	1	0	0	0	0	0	0	0	0	S_{12}
	0	0	0	0	0	0	1	-1	-1	0	0	0	0	0	0	0	0	0	0	0	S_{13}
	0	0	0	0	0	0	0	1	0	0	0	-1	1	0	-1	1	0	0	0	0	S_{14}
	0	0	0	0	0	0	0	0	1	-1	-1	0	0	0	0	0	0	0	0	0	S_{15}
	0	0	0	0	0	0	0	0	0	0	0	1	0	0	0	1	-1	-1	1	0	S_{16}
	0	0	0	0	0	0	0	0	0	0	0	0	0	-1	1	1	0	0	0	0	S_{17}
	0	0	0	0	0	0	0	0	0	0	0	0	1	-1	-1	0	0	0	0	0	S_{18}
	0	0	0	0	0	0	0	0	0	0	0	0	0	0	0	0	0	1	-1	0	S_{22}

Figure 2. Stoichiometric Matrix of the Reduced Hypoxia Response Network

The rows represent the 13 variable molecular species in Table 1, and the columns represent the 19 reactions in Table 2. doi:10.1371/journal.pcbi.0030171.g002

exactly matches the overall response and thus is responsible for it. For hypoxia, our analysis suggests that the cycle of abundant production and efficient degradation of HIF α plays the main role in the sharp response.

Results

Model Description

For consistency and ease of understanding, we use the notation and nomenclature in [1] and use their 23-species network and differential equation model as the starting point. With this background, the original network shown in Figure 2 of [1] can be further reduced in the following way. Kohn et al. [1] have shown that the feedback of mRNA is not necessary for the switch-like behavior. We therefore eliminate this feedback loop (reaction k_{32}). Hence, Transcript intermediate 1, 2, and 3 (Species 8, 9, and 10) can also be dropped, as well as the associated reactions: k_7 , k_8 , k_9 , k_{10} , and k_{11} , because they do not affect the dynamics of the network. Species 23 is only the joint name of HIF α :ARNT:HRE (Species 7) and HIF α OH:ARNT:HRE (Species 22); therefore, it is dropped. HIF α precursor (Species 1) is a constant and is thus dropped, because its information can be simply encoded in the reaction k_1 . The degradation products (Species 2) are also eliminated because they are assumed to leave the network immediately after their production and do not affect the dynamics. Similarly, species 19, 20, and 21 do not contribute to the dynamics and are therefore removed. The resulting network is summarized in Tables 1 and 2, where there are 13 molecular species and 19 reactions in total. The system can be described by the following set of ODEs where $[S_n]$ stands for the concentration of species n as tabulated in Table 1 and $[O_2]$ indicates the input cellular oxygen concentration. Table 2 shows the specific reaction each rate constants k_n represents. The real values of k_n are from [1]. Note that the ODE system below is typical: the terms are based on mass-action principles and, taken together, result in complex behavior not readily discernible by examining the equations. We also dropped the precursor concentration $[S_1]$ since it is set to unity.

$$\frac{d[S_3]}{dt} = k_1 - k_2[S_3] - k_{12}[S_3][S_{12}] + k_{13}[S_{13}] - k_3[S_3][S_4] + k_4[S_5] \quad (1)$$

$$\frac{d[S_4]}{dt} = -k_3[S_3][S_4] + k_4[S_5] + k_{22}[S_{16}] - k_{21}[S_4][S_{14}] \quad (2)$$

$$\begin{aligned} \frac{d[S_5]}{dt} = & k_3[S_3][S_4] - k_4[S_5] - k_5[S_5][S_6] + k_6[S_7] \\ & - k_{15}[S_5][S_{12}] + k_{16}[S_{15}] \end{aligned} \quad (3)$$

$$\frac{d[S_6]}{dt} = -k_5[S_5][S_6] + k_6[S_7] - k_{29}[S_{16}][S_6] + k_{30}[S_{22}] \quad (4)$$

$$\frac{d[S_7]}{dt} = k_5[S_5][S_6] - k_6[S_7] \quad (5)$$

$$\begin{aligned} \frac{d[S_{12}]}{dt} = & -k_{12}[S_3][S_{12}] + (k_{13} + k_{14}[O_2])[S_{13}] \\ & - k_{15}[S_5][S_{12}] + (k_{16} + k_{17}[O_2])[S_{15}] \end{aligned} \quad (6)$$

$$\frac{d[S_{13}]}{dt} = k_{12}[S_3][S_{12}] - (k_{13} + k_{14}[O_2])[S_{13}] \quad (7)$$

$$\begin{aligned} \frac{d[S_{14}]}{dt} = & k_{14}[O_2][S_{13}] - k_{18}[S_{14}][S_{17}] + k_{19}[S_{18}] \\ & - k_{21}[S_{14}][S_4] + k_{22}[S_{16}] \end{aligned} \quad (8)$$

$$\frac{d[S_{15}]}{dt} = k_{15}[S_5][S_{12}] - (k_{16} + k_{17}[O_2])[S_{15}] \quad (9)$$

$$\begin{aligned} \frac{d[S_{16}]}{dt} = & k_{17}[O_2][S_{15}] + k_{21}[S_4][S_{14}] \\ & - k_{22}[S_{16}] - k_{29}[S_{16}][S_6] + k_{30}[S_{22}] \end{aligned} \quad (10)$$

$$\frac{d[S_{17}]}{dt} = -k_{18}[S_{14}][S_{17}] + (k_{19} + k_{20})[S_{18}] \quad (11)$$

$$\frac{d[S_{18}]}{dt} = k_{18}[S_{14}][S_{17}] - (k_{19} + k_{20})[S_{18}] \quad (12)$$

$$\frac{d[S_{22}]}{dt} = k_{29}[S_{16}][S_6] - k_{30}[S_{22}] \quad (13)$$

Table 1. Molecular Species of the Reduced Network

Species Number	Initial Concentration	Species Identifier	Accession Number
S_3	5	HIF α	Q16665
S_4	5	ARNT	P27540
S_5	0	HIF α :ARNT	
S_6	1	HRE	
S_7	0	HIF α :ARNT:HRE	
S_{12}	10	PHD	Q96KS0, Q9H6Z9, Q9GZT9
S_{13}	0	HIF α :PHD	
S_{14}	0	HIF α OH	
S_{15}	0	HIF α :ARNT:PHD	
S_{16}	0	HIF α OH:ARNT	
S_{17}	10	VHL	I38926
S_{18}	0	HIF α OH:VHL	
S_{22}	0	HIF α OH:ARNT:HRE	
S_1	1	HIF precursor	
S_{20}	0.0–1.2	Oxygen	

There are 13 molecular species as the dynamical variables. In addition, there are two constant variables: S_1 for an HIF precursor whose concentration is fixed at unity ($[S_1] = 1$) and S_{20} for cellular oxygen whose concentration is set at different values to model the effect of its availability on the network ($[S_{20}] = [O_2] = 0.0 - 1.2$).
doi:10.1371/journal.pcbi.0030171.t001

Network Decomposition by Extreme Pathway Analysis

This section assumes some familiarity with linear algebra. The 13×19 stoichiometric matrix Φ of the reduced hypoxia response network (Tables 1 and 2) is shown in Figure 2 (for details, see Materials and Methods). The rank of Φ is computed and shown to be 9, indicating that there are only nine independent molecular species to serve as constraints for the analysis. Therefore, the dimension of the corresponding null space is 10. The linearly independent basis B vectors are generated by Matlab 6.5 and are shown in Figure 3. According to the constraint that no negative values are allowed in the basis vectors, we can uniquely transform basis B into basis P as shown in Figure 4. Both \mathbf{b}_8 and \mathbf{b}_9 have negative terms. \mathbf{b}_8 has to be transformed first, otherwise there will be no +1 to cancel out the -1 at the twelfth row of \mathbf{b}_8 . Each -1 in \mathbf{b}_8 is canceled out through the operation $\mathbf{b}_8 + \mathbf{b}_9$. In the second step, one has to use \mathbf{b}_7 to cancel -1 at the ninth row of \mathbf{b}_9 . In this way, we obtain the set of basis vectors P . The above analysis indicates that the dimension of this null space is the same as the number of edges for its corresponding convex cone [28], which is the algebraic basis for extreme pathways [14] and elementary modes [29].

The ten basis vectors of P represent ten underlying pathways of the hypoxia network. They are illustrated in Figures 5 and 6, from which one finds two distinct patterns: \mathbf{p}_1 , \mathbf{p}_7 , and \mathbf{p}_9 belong to the HIF α degradation pathways (Figure 5) and the others belong to the simple association-dissociation pathways (Figure 6). More specifically, through \mathbf{p}_1 , HIF α is directly degraded by reaction k_2 , a presumably oxygen-independent degradation pathway; whereas in oxygen-dependent pathways \mathbf{p}_7 and \mathbf{p}_9 , the hydroxylated HIF α is recognized by the VHL that channels it through a ubiquitin degradation component that is shown as the dotted box in Figure 5. Even though \mathbf{p}_1 , \mathbf{p}_7 , and \mathbf{p}_9 are all elementary modes [29], they can share certain reactions of the network. For example, the total influx for HIF α synthesis from a precursor can thus be decomposed into three parts with the overall rate

Table 2. 19 Reactions of the Reduced Network and Corresponding Reactants and Products

Reaction	Reactants	Products
k_1	S_1	S_3
k_2	S_3	
k_3	S_3 S_4	S_5
k_4	S_5	S_3 S_4
k_5	S_5 S_6	S_7
k_6	S_7	S_5 S_6
k_{12}	S_3 S_{12}	S_{13}
k_{13}	S_{13}	S_3 S_{12}
k_{14}	S_{13} S_{20}	S_{12} S_{14}
k_{15}	S_5 S_{12}	S_{15}
k_{16}	S_{15}	S_5 S_{12}
k_{17}	S_{15} S_{20}	S_{12} S_{16}
k_{18}	S_{14} S_{17}	S_{18}
k_{19}	S_{18}	S_{14} S_{17}
k_{20}	S_{18}	S_{17}
k_{21}	S_4 S_{14}	S_{16}
k_{22}	S_{16}	S_4 S_{14}
k_{29}	S_6 S_{16}	S_{22}
k_{30}	S_{22}	S_6 S_{16}

Note that k_2 represents a presumably oxygen-independent direct degradation process of HIF (S_3).
doi:10.1371/journal.pcbi.0030171.t002

constant k_1 being given by $\gamma_1 k_1$, $\gamma_2 k_1$, and $\gamma_3 k_1$, where $\gamma_1 + \gamma_2 + \gamma_3 = 1$.

The pathways \mathbf{p}_7 , and \mathbf{p}_9 are almost the same. The only difference is that HIF α is associated with ARNT in the middle part of the pathway \mathbf{p}_9 . Therefore, ARNT must be functionally very important, otherwise it would be hard to explain why the two underlying pathways, which should play significantly different roles, look so similar. Indeed, HIF α degrades differently through the two pathways. The k-sets were selected in [1] on the basis that they produced a switch-like behavior. For all the three k-sets, it was observed that HIF α has high affinity to PHD and low affinity to ARNT. The former is consistent with the usual case of high enzyme-substrate binding affinity. This implies that \mathbf{p}_9 is not the major degradation pathway because HIF α does not bind with ARNT very well. Moreover, \mathbf{p}_9 is immediately adjacent to HRE, which suggests its major role is to deliver signals to activate the promoters of hypoxia-regulated genes. As a signal transducer, the rate constant $\gamma_3 k_1$ itself need not to be high; what the downstream genes are sensitive to is $d(\gamma_3 k_1)/dt$. Therefore, we hypothesize that there is a negligible flux through \mathbf{p}_9 (or $\gamma_3 \approx 0$). To verify our hypothesis, we calculate the γ_1 , γ_2 , and γ_3 values, as the indication of the relative importance of \mathbf{p}_1 , \mathbf{p}_7 , and \mathbf{p}_9 in HIF α degradation, at different oxygen levels. The results are given in Table 3. Note that $[O_2] = 0.1$ and $[O_2] = 1.0$ represent typical low and high oxygen levels according to [1]. One sees that the pathway \mathbf{p}_9 is always much less important than the other two as far as HIF α degradation is concerned. The majority of HIF α gets degraded via either \mathbf{p}_1 at low oxygen or \mathbf{p}_7 at high oxygen. The comparison of hypoxia response network and heat shock response network [30] as in Table 4 shows the similarity between these two networks with respect to the issue of affinity. The huge difference in the affinity can clearly separate the underlying pathways and assign different

$$\mathcal{B} = \{\mathbf{b}_1, \dots, \mathbf{b}_{10}\} = \begin{pmatrix} 1 & 0 & 0 & 0 & 0 & 0 & 1 & 0 & 0 & 0 \\ 1 & 0 & 0 & 0 & 0 & 0 & 0 & 0 & 0 & 0 \\ 0 & 1 & 0 & 0 & 0 & 0 & 0 & -1 & 1 & 0 \\ 0 & 1 & 0 & 0 & 0 & 0 & 0 & 0 & 0 & 0 \\ 0 & 0 & 1 & 0 & 0 & 0 & 0 & 0 & 0 & 0 \\ 0 & 0 & 1 & 0 & 0 & 0 & 0 & 0 & 0 & 0 \\ 0 & 0 & 0 & 1 & 0 & 0 & 1 & 1 & -1 & 0 \\ 0 & 0 & 0 & 1 & 0 & 0 & 0 & 0 & 0 & 0 \\ 0 & 0 & 0 & 0 & 0 & 0 & 1 & 1 & -1 & 0 \\ 0 & 0 & 0 & 0 & 1 & 0 & 0 & -1 & 1 & 0 \\ 0 & 0 & 0 & 0 & 1 & 0 & 0 & 0 & 0 & 0 \\ 0 & 0 & 0 & 0 & 0 & 0 & 0 & -1 & 1 & 0 \\ 0 & 0 & 0 & 0 & 0 & 1 & 1 & 0 & 0 & 0 \\ 0 & 0 & 0 & 0 & 0 & 1 & 0 & 0 & 0 & 0 \\ 0 & 0 & 0 & 0 & 0 & 0 & 1 & 0 & 0 & 0 \\ 0 & 0 & 0 & 0 & 0 & 0 & 0 & 1 & 0 & 0 \\ 0 & 0 & 0 & 0 & 0 & 0 & 0 & 0 & 1 & 0 \\ 0 & 0 & 0 & 0 & 0 & 0 & 0 & 0 & 0 & 1 \\ 0 & 0 & 0 & 0 & 0 & 0 & 0 & 0 & 0 & 1 \end{pmatrix}$$

Figure 3. Set of Theoretically Feasible Basis Vectors **B**
doi:10.1371/journal.pcbi.0030171.g003

functions to them. This is also the basis for the Goldbeter-Koshland model [31]. We tested our method to all three parameter sets (k-sets 1, 2, and 3) in [1], and find that the analytical results are almost identical with those of the direct simulations of the entire network, which strongly validates our approximation. For the rest of the paper thereafter, we only report numerical results for k-set 1.

Analytical Solution to the Decomposed Hypoxia Response Network

The EPA method gives us a starting point from which to analyze our reaction network in greater and more revealing detail. The verification of our hypothesis implies that the pathways associated with \mathbf{p}_9 could be neglected in the first place. The following equations describe the combination \mathbf{p}_1 , \mathbf{p}_4 , \mathbf{p}_6 , and \mathbf{p}_7 , which constitute the oxygen sensing mechanism:

$$\frac{d[S_3]}{dt} = k_1 - k_2[S_3] - k_{12}[S_3][S_{12}] + k_{13}[S_{13}], \quad (14)$$

$$\frac{d[S_{12}]}{dt} = -k_{12}[S_3][S_{12}] + k_{13}[S_{13}] + k_{14}[O_2][S_{13}], \quad (15)$$

$$\frac{d[S_{13}]}{dt} = k_{12}[S_3][S_{12}] - k_{13}[S_{13}] - k_{14}[O_2][S_{13}], \quad (16)$$

$$\frac{d[S_{14}]}{dt} = k_{14}[O_2][S_{13}] - k_{18}[S_{14}][S_{17}] + k_{19}[S_{18}], \quad (17)$$

$$\frac{d[S_{17}]}{dt} = -k_{18}[S_{14}][S_{17}] + k_{19}[S_{18}] + k_{20}[S_{18}], \quad (18)$$

$$\frac{d[S_{18}]}{dt} = k_{18}[S_{14}][S_{17}] - k_{19}[S_{18}] - k_{20}[S_{18}]. \quad (19)$$

Note the differences between Equations 1, 6, and 8, and Equations 14, 15, and 17. The \mathbf{p}_9 related elements have been omitted due to their smallness. By setting the left-hand sides

$$\mathcal{P} = \left. \begin{matrix} \mathbf{p}_1 = \mathbf{b}_1 \\ \mathbf{p}_2 = \mathbf{b}_2 \\ \mathbf{p}_3 = \mathbf{b}_3 \\ \mathbf{p}_4 = \mathbf{b}_4 \\ \mathbf{p}_5 = \mathbf{b}_5 \\ \mathbf{p}_6 = \mathbf{b}_6 \\ \mathbf{p}_7 = \mathbf{b}_7 \\ \mathbf{p}_8 = \mathbf{b}_8 + \mathbf{b}_9 \\ \mathbf{p}_9 = \mathbf{b}_9 + \mathbf{b}_7 \\ \mathbf{p}_{10} = \mathbf{b}_{10} \end{matrix} \right\} = \begin{pmatrix} 1 & 0 & 0 & 0 & 0 & 0 & 1 & 0 & 1 & 0 \\ 1 & 0 & 0 & 0 & 0 & 0 & 0 & 0 & 0 & 0 \\ 0 & 1 & 0 & 0 & 0 & 0 & 0 & 0 & 1 & 0 \\ 0 & 1 & 0 & 0 & 0 & 0 & 0 & 0 & 0 & 0 \\ 0 & 0 & 1 & 0 & 0 & 0 & 0 & 0 & 0 & 0 \\ 0 & 0 & 1 & 0 & 0 & 0 & 0 & 0 & 0 & 0 \\ 0 & 0 & 0 & 1 & 0 & 0 & 1 & 1 & 0 & 0 \\ 0 & 0 & 0 & 0 & 0 & 0 & 1 & 1 & 0 & 0 \\ 0 & 0 & 0 & 0 & 1 & 0 & 0 & 0 & 1 & 0 \\ 0 & 0 & 0 & 0 & 1 & 0 & 0 & 0 & 0 & 0 \\ 0 & 0 & 0 & 0 & 0 & 0 & 0 & -1 & 1 & 0 \\ 0 & 0 & 0 & 0 & 0 & 1 & 1 & 0 & 0 & 0 \\ 0 & 0 & 0 & 0 & 0 & 1 & 0 & 0 & 0 & 0 \\ 0 & 0 & 0 & 0 & 0 & 0 & 1 & 0 & 0 & 0 \\ 0 & 0 & 0 & 0 & 0 & 0 & 0 & 1 & 0 & 1 \\ 0 & 0 & 0 & 0 & 0 & 0 & 0 & 1 & 1 & 0 \\ 0 & 0 & 0 & 0 & 0 & 1 & 0 & 0 & 0 & 0 \\ 0 & 0 & 0 & 0 & 0 & 0 & 1 & 0 & 1 & 0 \\ 0 & 0 & 0 & 0 & 0 & 0 & 0 & 1 & 0 & 0 \\ 0 & 0 & 0 & 0 & 0 & 0 & 0 & 0 & 0 & 1 \\ 0 & 0 & 0 & 0 & 0 & 0 & 0 & 0 & 0 & 1 \end{pmatrix}$$

Figure 4. Set of Both Theoretically and Biochemically Feasible Basis Vectors **P**
doi:10.1371/journal.pcbi.0030171.g004

of the above equations to zero, one obtains the steady state equations:

$$k_1 - k_2[S_3^*] - k_{12}[S_3^*][S_{12}^*] + k_{13}[S_{13}^*] = 0, \quad (20)$$

$$k_{12}[S_3^*][S_{12}^*] - k_{13}[S_{13}^*] - k_{14}[O_2][S_{13}^*] = 0, \quad (21)$$

$$k_{14}[O_2][S_{13}^*] - k_{18}[S_{14}^*][S_{17}^*] + k_{19}[S_{18}^*] = 0, \quad (22)$$

$$k_{18}[S_{14}^*][S_{17}^*] - k_{19}[S_{18}^*] - k_{20}[S_{18}^*] = 0. \quad (23)$$

The total amount of PHD is conserved: PHD is either in the form of PHD (S_{12}) or HIF α :PHD (S_{13}). This implies

$$[S_{13}^*] + [S_{12}^*] = [S_{12}^0], \quad (24)$$

where $[S_{12}^0]$ is the initial concentration of PHD. By some derivation, the following equation is obtained:

$$a[S_3^{*2}] + b[S_3^*] + c = 0, \quad (25)$$

where $a = k_2k_{12}$, $b = b_1 + b_2[O_2]$, $c = c_1 + c_2[O_2]$, where

$$b_1 = k_{13}k_2 - k_1k_{12},$$

$$b_2 = k_{12}k_{14}[S_{12}^0] + k_2k_{14},$$

$$c_1 = -k_1k_{13},$$

$$c_2 = -k_1k_{14}.$$

Since $c < 0$, Equation 25 has one and only one reasonable root

$$[S_3^*] = (\sqrt{b^2 - 4ac} - b)/2a \quad (26)$$

Note that none of the species and reactions in the degradation box is present in Equation 26, which indicates that the components in the degradation box are not

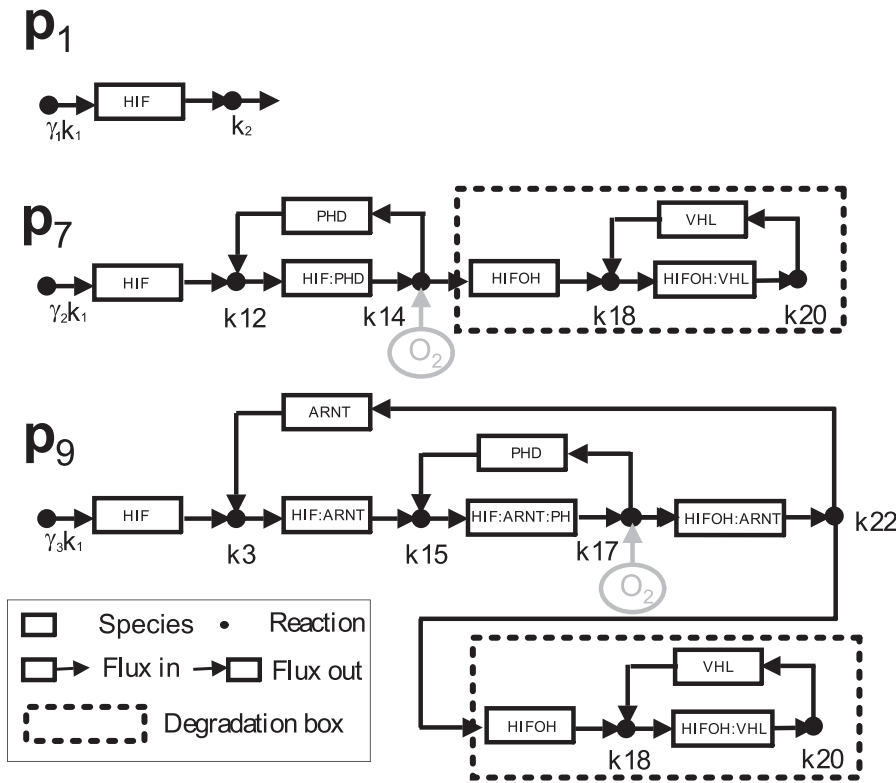


Figure 5. Graphical Representations of the Three Underlying Pathways of HIF α Degradation: \mathbf{p}_1 , \mathbf{p}_7 , and \mathbf{p}_9 . Through \mathbf{p}_1 , HIF α is degraded directly by k_2 . In \mathbf{p}_7 , HIF α first binds with PHD after synthesis. HIF α :PHD is then dissociated into PHD and HIF α OH with the participation of oxygen. HIF α OH then binds with VHL to form HIF α OH:VHL. Finally, the dissociation of HIF α OH:VHL concludes HIF α degradation. The pathway \mathbf{p}_9 differs from \mathbf{p}_7 only in that HIF α first binds with ARNT after synthesis. doi:10.1371/journal.pcbi.0030171.g005

responsible for the sharp response curve. Once $[S_3^*]$ is determined, the analysis of the remaining network (\mathbf{p}_2 , \mathbf{p}_3 , \mathbf{p}_5 , \mathbf{p}_6 , \mathbf{p}_8 , \mathbf{p}_9 , and \mathbf{p}_{10}) becomes straightforward, and the results are given in the section “Additional results.” In fact, these results can be further simplified (see Equations 30 and 43 for $[S_3^*]$ and $[S_7^*]$).

Figure 7A and 7B shows the steady-state values of $[HIF\alpha]$ ($[S_3^*]$) and $[HIF\alpha:ARNT:HRE]$ ($[S_7^*]$) at different oxygen values. The red lines depict the simulation results obtained by the numerical integration of the ODE system (1–13) until the steady state is reached. The black lines depict the analytical solutions that are obtained by the algebraic Equations 26 and 56. To better determine the critical point of pathway switching, we calculate $\partial[S_3^*]/\partial[O_2]$ and $\partial[S_7^*]/\partial[O_2]$. The results are shown in Figure 7C and 7D. One sees that both $\partial[S_3^*]/\partial[O_2]$ and $\partial[S_7^*]/\partial[O_2]$ change abruptly in a very narrow region of $[O_2]$, with the rest of the values almost zero. One observes that the critical point is about $[O_2]^c = 0.65$.

We thus show that the sharpness of the response curve can be determined analytically, instead of exhaustively enumerating $[O_2]$ values combined with time-consuming numerical integration of a large number of ODEs at each $[O_2]$ value.

Discussion

EPA is a powerful, yet simple tool that can significantly reduce the complexity of the original network and thus make further analytical effort feasible. In this paper, the additional analysis explains precisely the sharp reaction to oxygen of the

network as a whole. The clear separation of \mathbf{p}_7 and \mathbf{p}_9 indicates their different functions: the pathway \mathbf{p}_7 and its other associated pathways constitute the sensing of ambient molecular oxygen; in contrast, the pathway \mathbf{p}_9 and its associated other pathways are responsible for the signal transduction to form the promoters of hypoxia-regulated genes. Most importantly, the simplification allows for a complete explanation of the switch behavior and a clear presentation of the relations between $[S_3^*]$ and $[O_2]$, $[S_7^*]$ and $[O_2]$, $[S_3^*]$ and $[S_7^*]$. The first step below explains the sharp HIF α stabilization. The second step explains the sharp HRE occupancy that is induced by the HIF α stabilization.

HIF α stabilization. This involves the dissociation of pathways \mathbf{p}_1 , \mathbf{p}_4 , \mathbf{p}_6 , and \mathbf{p}_7 from the whole network, due to the fact that the flux through \mathbf{p}_9 is always small and can be neglected. It reveals a critical value that corresponds to the switching between pathways \mathbf{p}_1 and \mathbf{p}_7 . Since an abrupt change often relates to the notion of singularity in mathematics, we proceed to see if a singularity can be found. Under normoxia, $[S_3^*] \approx 0$, and $a[S_3^*]^2$ can be neglected in Equation 25, which yields

$$[S_3^*] = -\frac{c}{b} = -\frac{c_1 + c_2[O_2]}{b_1 + b_2[O_2]} \quad (27)$$

One immediately finds the singularity

$$[O_2]^c = -b_1/b_2 \quad (28)$$

For k-set 1 in [1], one obtains $[O_2]^c = 0.64$, which is exactly the critical value found in Figure 7. When the oxygen level

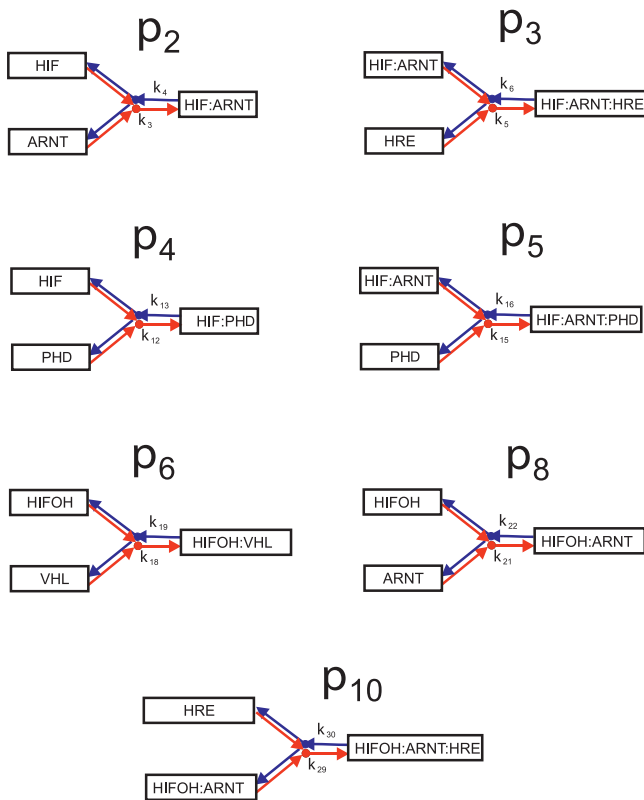


Figure 6. Simple Association and Dissociation pathways p_2 , p_3 , p_4 , p_5 , p_6 , p_8 , and p_{10} . The associations (dissociations) are illustrated in red (blue). doi:10.1371/journal.pcbi.0030171.g006

decreases to a value close to $[O_2]^c$, the denominator in Equation 27 becomes very small and $a [S_3^*]^2$ can no longer be ignored. Moreover, the term c in Equation 25 can be ignored compared with the large value of $[S_3^*]$. One thus has

$$[S_3^*] = -\frac{b}{a} = -\frac{b_1}{a} - \frac{b_2}{a} [O_2] = \frac{b_2}{a} ([O_2]^c - [O_2]) \quad (29)$$

This explains the linear decrease of $[S_3^*]$ versus $[O_2]$ increasing in Figure 7A. In summary, one has

$$[S_3^*] = \begin{cases} -c/b & [O_2] > [O_2]_+^c \\ -b/a & [O_2] < [O_2]_-^c \end{cases} \quad (30)$$

One can check that k_2 can be ignored in the upper branch of Equation 30 due to its smallness, which again demonstrates that the pathway p_1 is not important under normoxia. The very smallness of k_2 reflects the importance of p_1 under hypoxia, for k_2 exists at the denominator of the lower branch of Equation 30.

HRE occupancy. The remaining pathways reveal how HIF α stabilization triggers a sharp increase of HIF α :ARNT:HRE, namely the sigmoid curve of $[S_7^*]$ versus $[O_2]$. We conclude that the magnitude of HIF α is crucial for the sharpness of the curve. To show this, we need Equations 47, 48, 53, and 54. By removing the terms that are negligible, these equations turn into

$$k_3 [S_3^*] [S_4^*] - k_4 [S_5^*] = 0, \quad (31)$$

Table 3. Flux through Pathways p_1 , p_7 , and p_9 at $[O_2] = 0.1$ and $[O_2] = 1.0$ for the Three Sets of Parameters Given in [1]

Pathways		$p_1(\gamma_1)$	$p_7(\gamma_7)$	$p_9(\gamma_9)$
k-set 1	$[O_2] = 0.1$	84.45%	15.20%	0.35%
	$[O_2] = 1.0$	0.09%	97.69%	2.22%
k-set 2	$[O_2] = 0.1$	86.72%	13.14%	0.14%
	$[O_2] = 1.0$	0.10%	98.97%	0.93%
k-set 3	$[O_2] = 0.1$	88.20%	11.58%	0.22%
	$[O_2] = 1.0$	0.08%	97.18%	2.74%

For high (low) oxygen level, HIF α is mainly degraded through pathway p_7 (p_1). doi:10.1371/journal.pcbi.0030171.t003

$$k_5 [S_5^*] [S_6^*] - k_6 [S_7^*] = 0, \quad (32)$$

$$[S_6^*] + [S_7^*] = [S_6^0], \quad (33)$$

$$[S_4^*] + [S_5^*] + [S_7^*] = [S_4^0]. \quad (34)$$

Equation 31 holds because $k_{15} [S_5^*] [S_{12}^*]$ and $k_{16} [S_{15}^*]$ are far less than $k_3 [S_3^*] [S_4^*]$ and $k_4 [S_5^*]$. Equation 33 holds because $[S_{22}^*]$ is far less than $[S_6^*]$ and $[S_7^*]$. Equation 34 holds because $[S_{15}^*]$, $[S_{16}^*]$, and $[S_{22}^*]$ are far less than $[S_4^*]$, $[S_5^*]$, and $[S_7^*]$. The validity of the above approximations can be easily checked. For example, for $[O_2] = 0.1$, one finds $k_3 [S_3^*] [S_4^*] = k_4 [S_5^*] = 1.66$, $k_{15} [S_5^*] [S_{12}^*] = k_{16} [S_{15}^*] = 0.005$, $[S_4^*] = 1.19$, $[S_5^*] = 2.69$, $[S_6^*] = 0.11$, $[S_7^*] = 0.89$, $[S_{15}^*] = 0.23$, $[S_{16}^*] = 0.0016$, and $[S_{22}^*] = 0.0005$. From Equations 31–34, one obtains

$$[S_7^*]^2 - \alpha [S_7^*] + [S_4^0] [S_6^0] = 0, \quad (35)$$

where $\alpha = \alpha_1 + \alpha_2 / [S_3^*]$, $\alpha_1 = [S_4^0] + [S_6^0] + k_6 / k_5$, and $\alpha_2 = k_4 k_6 / (k_3 k_5)$. $[S_7^*]$ has one and only one reasonable solution

$$[S_7^*] = \frac{2[S_4^0][S_6^0]}{\alpha + \sqrt{\alpha^2 - 4[S_4^0][S_6^0]}} = \frac{2[S_4^0][S_6^0]}{\alpha + \alpha\sqrt{1 - x^2}}, \quad (36)$$

where $x = 2 [S_4^0][S_6^0] / \alpha$. Taylor expanding $\sqrt{1 - x^2}$, yields

$$\sqrt{1 - x^2} = 1 - x^2/2 + x^4/8 + O(x^6).$$

No matter what $[S_3^*]$ value is, $x < 2 [S_4^0][S_6^0] / \alpha_1 = 0.74$, so $1 - x^2/2 > 0.73$ and $x^4/8 < 0.0375$. Therefore $\sqrt{1 - x^2} \approx 1 - x^2/2$ and

$$[S_7^*] \approx \frac{[S_4^0][S_6^0]}{\alpha - [S_4^0][S_6^0] / \alpha}. \quad (37)$$

Under normoxia $[S_3^*]$ is small, so $\alpha \approx \alpha_2 / [S_3^*]$ and $1/\alpha \approx 0$. From Equation 37 one has

$$[S_7^*] \approx [S_4^0][S_6^0][S_3^*] / \alpha_2. \quad (38)$$

which is also small. Under hypoxia, $[S_3^*]$ is large, and thus

$$\frac{1}{\alpha} = \frac{1/\alpha_1}{1 + \alpha_2 / (\alpha_1 [S_3^*])} \approx \frac{1}{\alpha_1} \left(1 - \frac{\alpha_2 / \alpha_1}{[S_3^*]} \right). \quad (39)$$

By substituting Equation 39 into Equation 37, one obtains the important relation between $[S_3^*]$ and $[S_7^*]$:

Table 4. Comparison between Hypoxia Response Network and Heat Shock Response Network

Hypoxia	Heat Shock	Characteristic
HIF α	σ^{32}	Key element
PHD	DnaK	High affinity
ARNT	RNAP	Low affinity

doi:10.1371/journal.pcbi.0030171.t004

$$[S_7^*] \approx \frac{[S_4^0][S_6^0]}{\beta_1} \left(1 - \frac{1}{1 + \beta_2[S_3^*]} \right), \quad (40)$$

where

$$\beta_1 = \frac{\alpha_1^2 - [S_4^0][S_6^0]}{\alpha_1}$$

and

$$\beta_2 = \frac{\alpha_1 \alpha_1^2 - [S_4^0][S_6^0]}{\alpha_2 \alpha_1^2 + [S_4^0][S_6^0]}.$$

By substituting Equation 29 into Equation 40, one obtains

$$[S_7^*] = m \left(1 - \frac{1}{1 + \lambda([O_2]^c - [O_2])} \right), \quad (41)$$

where $m = [S_4^0][S_6^0]/\beta_1$ and $\lambda = \beta_2 b_2/a$. It is well-known that

Equation 41 represents a sigmoid curve with m controlling the saturation value and λ controlling the sharpness. By ignoring the small term k_6/k_5 in the expression of α_1 , one finds m is a function of $[S_4^0]$ and $[S_6^0]$ only. One also finds

$$\lambda = \frac{k_3 k_5 b_2}{k_4 k_6 a}. \quad (42)$$

Here

$$\bar{c} \approx \frac{[S_4^0]^2 + [S_6^0]^2 + [S_4^0][S_6^0]}{[S_4^0]^2 + [S_6^0]^2 + 3[S_4^0][S_6^0]} ([S_4^0] + [S_6^0]).$$

The association (disassociation) constants k_3, k_5 (k_4, k_6) exist in the numerator (denominator) of the term $k_3 k_5/(k_4 k_6)$, which implies that the higher the affinity, the sharper the response. The third term b_2/a is proportional to the HIF level. In summary, our analysis yields

$$[S_7^*] = \begin{cases} \text{Eq. (38)} & [O_2] > [O_2]^c_+ \\ \text{Eq. (41)} & [O_2] < [O_2]^c_- \end{cases} \quad (43)$$

One sees that HIF α is the key to triggering the HIF α :ARNT:HRE response. As long as the oxygen level is greater than $[O_2]^c$, HIF α is efficiently degraded by the pathway p_7 and maintains a very low level, and the HIF α :ARNT:HRE level is also low (Equation 38). When the oxygen level drops below $[O_2]^c$, the system switches to the pathway p_1 , and HIF α stabilizes with a large concentration (b_2/a large). This triggers the sharp increase of HIF α :ARNT:HRE. The smaller k_2 is, the larger b_2/a , and the sharper the HRE occupancy response (see

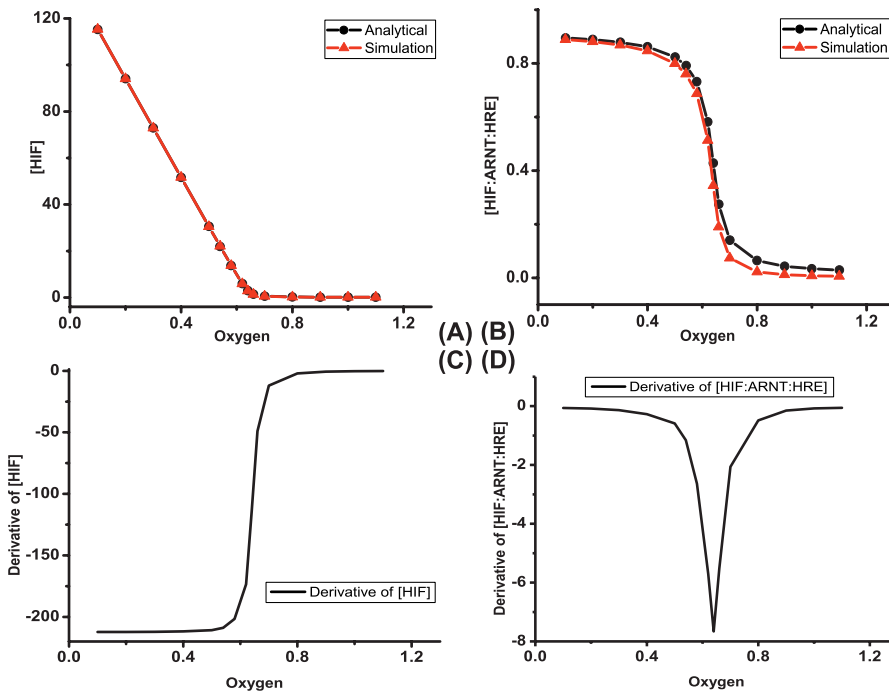


Figure 7. Steady State Values of [HIF α] and [HIF α :ARNT:HRE]

- (A) The comparison between analytical and numerical solutions of [HIF α].
- (B) The comparison between analytical and numerical solutions of [HIF α :ARNT:HRE].
- (C) The first derivative of [HIF α] with respect to $[O_2]$.
- (D) The first derivative of [HIF α :ARNT:HRE] with respect to $[O_2]$.

doi:10.1371/journal.pcbi.0030171.g007

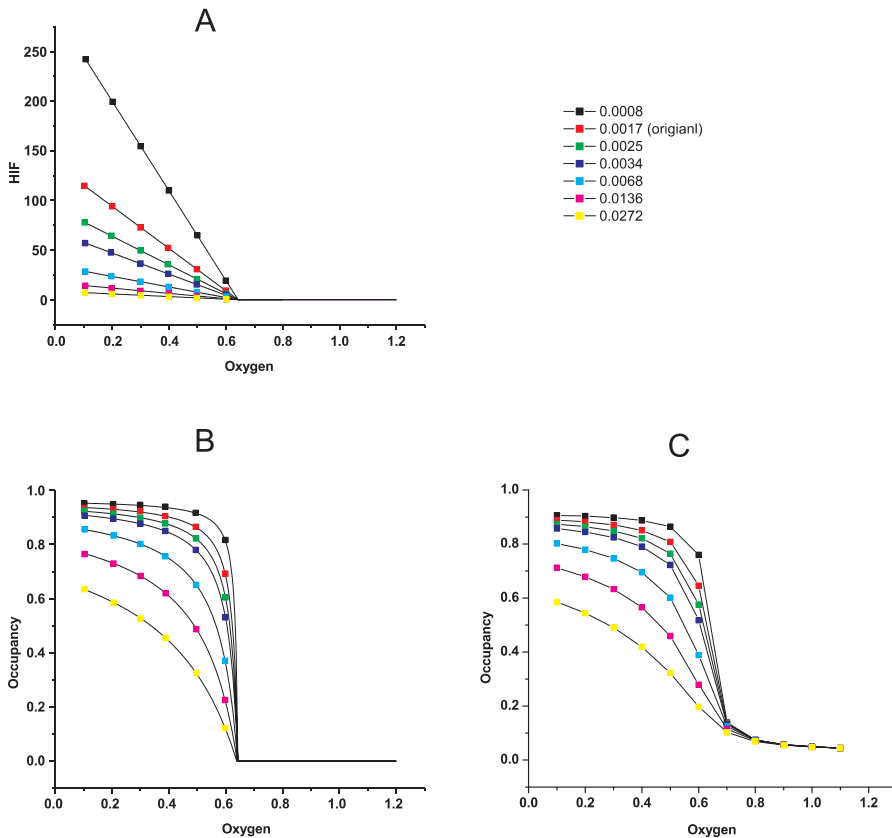


Figure 8. Different HIF and HRE Occupancy Responses at Different k_2 Values

(A) is obtained by the analytical solution Equation 29; (B) is obtained by the analytical solution Equation 41; (C) is obtained by the numerical integration of Equations 1–13; (A) and (B) reveal how HIF α controls HRE occupancy: the larger the HIF α level is, the sharper the HRE occupancy response. The validity of our analytical method is demonstrated by the close resemblance of (B) and (C).

doi:10.1371/journal.pcbi.0030171.g008

Figure 8). Also, the validity of our analytical approximation is justified by the close resemblance of Figure 8B and 8C.

The three major results of Kohn [1] involve HRE occupancy as a function of the oxygen concentration. The dependence of the curve on ARNT, VHL, and PHD are obtained by both simulation (Figure 9A) and analysis (Figure 9B) and are explained as follows.

ARNT dependence. We need only to analyze the pathway p_9 . The amount of ARNT does not affect the shape of the response curve or the location of the sharp transition, because p_9 is the pathway for HRE expression, while p_7 is responsible for the sharpness. HIF α :ARNT would not be generated without ARNT and there would not be expressions of HRE for any level of oxygen. At high oxygen levels, the concentrations are similar because HRE occupancy is low anyway. At low oxygen levels, low levels of ARNT will give low HIF α :ARNT and then low HRE occupancy.

VHL dependence. VHL is present in both p_7 and p_9 . At high oxygen levels, one should analyze p_7 because it is the major pathway for HIF α degradation. The VHL source will affect the upstream HIF α . If VHL concentration is low, it cannot degrade HIF α fast, and the system yields high HRE occupancy. At low oxygen levels, p_1 is the major pathway for HIF α degradation, which does not depend on VHL.

PHD dependence. One interesting property relates to the different locations of the transition. Using the criterion identified by the alternative model without reaction k_2 , we

can calculate the transition locations as shown in Figure 9B3 for different PHD values. The results are the same as in Figure 9A3. As a matter of fact, considering the p_9 pathway only yields a much simpler analytical solution that is also accurate. This further simplification is due to the fact that the expression of HIF α :OH:ARNT:HRE is always negligible.

The present model of the hypoxia response network is probably an oversimplified one. Nevertheless, it serves as an important starting point, from both theoretical and experimental perspectives, before a more detailed model can be understood. The present model will be gradually expanded and analyzed, with the input of more quantitative data from future experiments. One advantage of EPA is that the method can easily incorporate mechanistic details as soon as they become available [16]. There are various molecular interactions that can be added to the model. For example, it was demonstrated that HIF influences mitochondrial function by inducing pyruvate dehydrogenase kinase 1 (PDK1) to suppress the tricarboxylic acid (TCA) cycle and thus the aerobic respiration. Then the respiration shifts to be anaerobic, whereby the oxygen resource can be preserved to promote cell survival under hypoxic environment [32–34]. Another subject we are interested in is the inclusion of ROS in the network. It has been established that ROS affects HIF α degradation through Fe $^{2+}$ [7–10]. The direct hydroxylation of HIF α by oxygen requires Fe $^{2+}$. Under hypoxia conditions, however, ROS increases dramatically and consistently removes Fe $^{2+}$ via

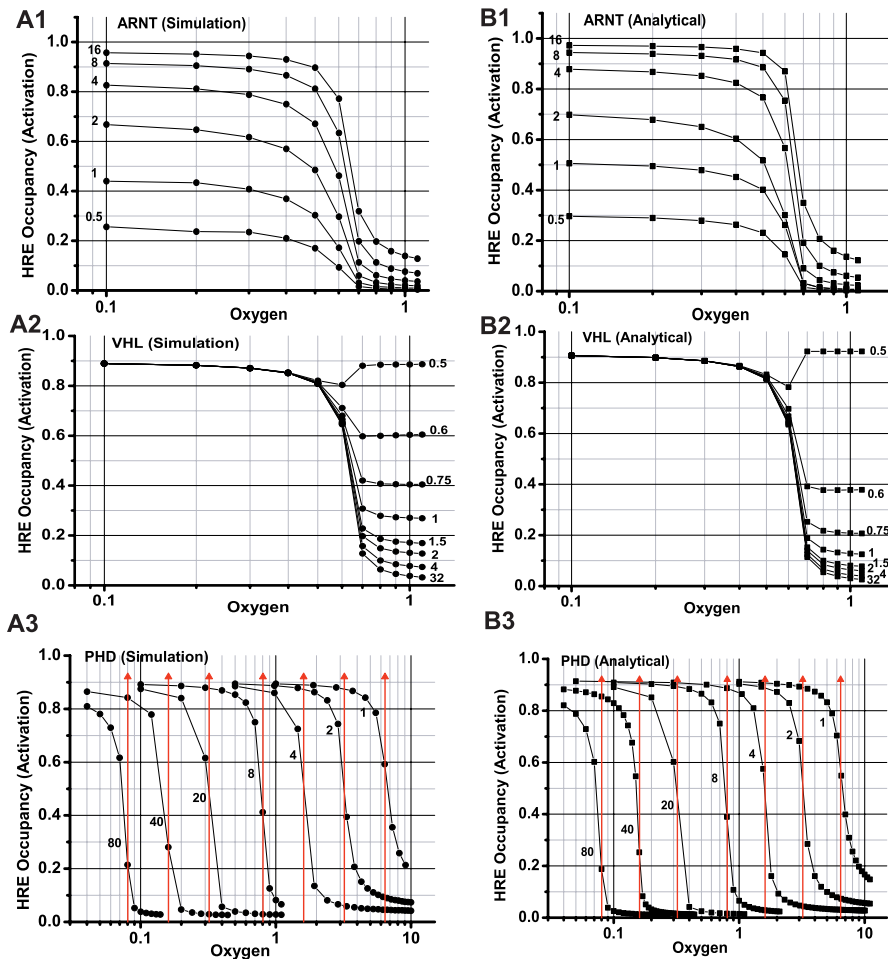


Figure 9. Dependence of the Oxygen Response Curves on the Amounts of Protein Components in the System
 The red lines in A3 and B3 represent the transition locations calculated from Equation 28.
 doi:10.1371/journal.pcbi.0030171.g009

oxidation to Fe^{3+} . Together with the shortage of oxygen, this makes the HIF α degradation through the VHL pathway even more difficult. Consequently, the transition would be faster and sharper. Analysis should focus on the explanation of the coexistence of two oxygen sensing components, a matter that does not appear to be settled as yet.

To obtain the dynamical response when the oxygen changes continuously in time, Equations 1–13 (the full model) are integrated. Figure 10 shows the temporal changes of [HIF α] and [HIF α :ARNT:HRE] as responses to the oxygen decreasing from 1.0 to 0.1 with different rates. One sees that $[S_3]$ and $[S_7]$ increase prominently only after $[O_2]$ decreases below $[O_2]^c$. The faster $[O_2]$ decreases, the more rapid the responses are. In particular, when $[O_2]$ abruptly jumps from 1.0 to 0.1, the responses ensue promptly. However, it is worth noting that one cannot tell practically how fast the responses are because the time scale is unknown. Indeed, the model is dimensionless and no units are given. Nevertheless, the sharp curves illustrate that the responses are very sensitive to the oxygen concentration and imply that the system can provide a timely response under hypoxia. Physiologists have long been puzzled by the ceaseless HIF α cycle, characterized by both abundant generation and efficient degradation, which seems to be a highly wasteful process. Our analysis provides a reasonable explanation. To deal with a sudden environmental change from normoxia to hypoxia, an organism must respond in time

to trigger the genes necessary for adapting to the new environment. To achieve such a sharp response, a high HIF α generation potential is necessary. Since the hypoxia conditions are rare, an efficient degradation pathway has to be designed to maintain a low HIF α under normoxia. The HIF α cycle is indeed uneconomic, but it appears useful in helping the cell respond to sudden, unpredictable changes in its environment.

In summary, we have obtained an accurate analytical solution to the hypoxia response network and have provided a complete explanation of the switch-like behavior first observed and modeled in [1]. The first step of our analysis applied the EPA technique to a reduced, yet complete system that resulted in exposing ten independent pathways, allowing us to focus on analyzing the pathways relevant to HRE occupancy. The analysis showed that the sharp response of HRE occupancy is due to the switch between the pathway p_7 (p_1) that degrades HIF α under normoxia (hypoxia).

Materials and Methods

In following the law of mass conservation, a particular reactant through each reaction can be written in the form of homogeneous linear equations,

$$\Phi \cdot \mathbf{v} = 0. \tag{44}$$

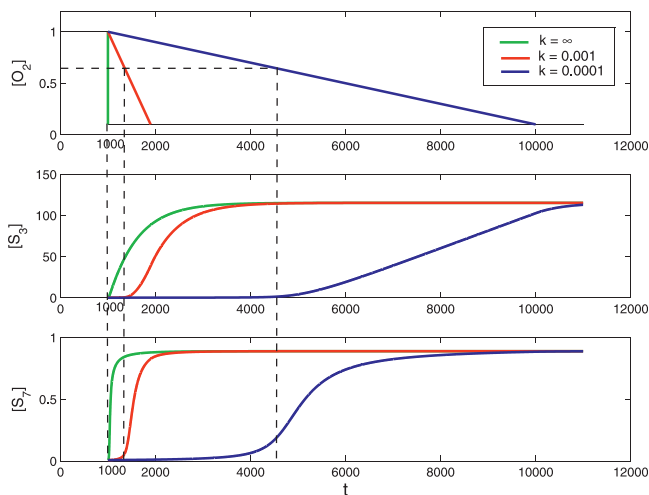


Figure 10. The Responses of $[S_3]$ and $[S_7]$ as the Oxygen Concentration Decreases from 1.0 to 0.1

The oxygen decreases linearly, $[O_2] = 1.0 - k_t$. The green, red, and blue lines correspond to the cases $k = \infty$ (abrupt decrease), $k = 0.001$, and $k = 0.0001$, respectively. The horizontal dotted line illustrates the critical point $[O_2]^c$. The vertical dotted lines show that the responses become prominent only after the oxygen concentration decreases below $[O_2]^c$. doi:10.1371/journal.pcbi.0030171.g010

Here Φ is an $m \times m$ stoichiometric matrix, where m is the number of metabolites and n is the number of reactions taking place within the network, with each element

$$\Phi_{ij} = \begin{cases} 1, & \text{if row } i \text{ is produced in column } j; \\ -1, & \text{if row } i \text{ is consumed in column } j; \\ 0, & \text{if row } i \text{ is not presented in column } j. \end{cases}$$

$\mathbf{v} = \sum_{k=1}^N f_k v_k$, where $N = \dim \text{Nul } \Phi$ is the dimension of the null space of Φ , v_k is the basis vector that corresponds to the k -th pathway, and f_k is the flux through the k -th pathway.

The determination of flux f_k requires numerical calculations. Note that v_k does not depend on f_k and can be obtained solely from Φ . That is, one can decompose the whole network into N elementary pathways without any ODE integration involved. The dimension of the null space of Φ follows the simple equation

$$\dim \text{Nul } \Phi + \text{rank } \Phi = n. \quad (45)$$

Using Matlab (<http://www.mathworks.com>), the rank of this 13×19 stoichiometric matrix Φ is found to be nine, and the dimension of the corresponding null space is thus ten. Also, a set (\mathbf{B}) of ten independent basis vectors is generated as shown in Figure 3. However, the set is not biologically reasonable due to the negative entries therein. By simple linear transformation, another set (\mathbf{P}) of ten vectors (Figure 4) is obtained whose entries are all non-negative (either 1 or 0) and are thus biologically feasible.

Additional results. The remaining network can be solved analytically with $\text{HIF}\alpha([S_3^*])$ already determined. The ODE description is as follows:

$$\frac{d[S_4]}{dt} = -k_3[S_3][S_4] + k_4[S_5] + k_{22}[S_{16}] - k_{21}[S_4][S_{14}]$$

$$\frac{d[S_5]}{dt} = k_3[S_3][S_4] - k_4[S_5] - k_5[S_5][S_6] + k_6[S_7] - k_{15}[S_5][S_{12}] + k_{16}[S_{15}]$$

$$\frac{d[S_6]}{dt} = -k_5[S_5][S_6] + k_6[S_7] - k_{29}[S_{16}][S_6] + k_{30}[S_{22}]$$

$$\frac{d[S_7]}{dt} = k_5[S_5][S_6] - k_6[S_7]$$

$$\frac{d[S_{22}]}{dt} = k_{29}[S_{16}][S_6] - k_{30}[S_{22}]$$

$$\frac{d[S_{15}]}{dt} = k_{15}[S_5][S_{12}] - (k_{16} + k_{17}[O_2])[S_{15}]$$

$$\frac{d[S_{16}]}{dt} = k_{17}[O_2][S_{15}] + k_{21}[S_4][S_{14}] - k_{22}[S_{16}]$$

$$\frac{d[S_{12}]}{dt} = -k_{12}[S_3][S_{12}] + (k_{13} + k_{14}[O_2])[S_{13}] - k_{15}[S_5][S_{12}] + (k_{16} + k_{17}[O_2])[S_{15}]$$

$$\frac{d[S_{13}]}{dt} = k_{12}[S_3][S_{12}] - (k_{13} + k_{14}[O_2])[S_{13}]$$

Together with the three constraints of $[S_4^0]$, $[S_6^0]$, and $[S_{12}^0]$, the steady state equations are expressed as follows:

$$-k_3[S_3^*][S_4^*] + k_4[S_5^*] + k_{22}[S_{16}^*] - k_{21}[S_4^*][S_{14}^*] = 0, \quad (46)$$

$$k_3[S_3^*][S_4^*] - k_4[S_5^*] - k_{15}[S_5^*][S_{12}^*] + k_{16}[S_{15}^*] = 0, \quad (47)$$

$$k_5[S_5^*][S_6^*] - k_6[S_7^*] = 0, \quad (48)$$

$$k_{29}[S_{16}^*][S_6^*] - k_{30}[S_{22}^*] = 0, \quad (49)$$

$$k_{15}[S_5^*][S_{12}^*] - k_{16}[S_{15}^*] - k_{17}[O_2][S_{15}^*] = 0, \quad (50)$$

$$k_{17}[O_2][S_{15}^*] + k_{21}[S_4^*][S_{14}^*] - k_{22}[S_{16}^*] = 0, \quad (51)$$

$$[S_{12}^*] + [S_{13}^*] + [S_{15}^*] = [S_{12}^0], \quad (52)$$

$$[S_6^*] + [S_7^*] + [S_{22}^*] = [S_6^0], \quad (53)$$

$$[S_4^*] + [S_5^*] + [S_7^*] + [S_{15}^*] + [S_{16}^*] + [S_{22}^*] = [S_4^0], \quad (54)$$

where $[S_3^*]$ and $[S_{14}^*]$ have already been determined from the analysis of \mathbf{p}_7 . By some reasoning, a quartic equation

$$J_1[S_5^*]^4 + J_2[S_5^*]^3 + J_3[S_5^*]^2 + J_4[S_5^*] + J_5 = 0 \quad (55)$$

is derived, from which $[S_5^*]$ can be obtained. $[S_7^*]$ and $[S_{22}^*]$ can then be expressed as functions of $[S_5^*]$:

$$\frac{1}{[S_7^*]} = \frac{F_1}{k_{22}E_3[S_6^0]} + \frac{F_2}{k_{22}E_3[S_6^0](E_2 + E_1[S_5^*])} + \frac{k_6}{k_5[S_6^0][S_5^*]}, \quad (56)$$

$$[S_{22}^*] = [S_6^0] - \frac{k_6[S_7^*]}{k_5[S_5^*]} - [S_7^*], \quad (57)$$

where

$$J_1 = H_1 E_1 I_1$$

$$J_2 = H_1 E_2 I_1 + H_1 E_1 I_2 + H_2 I_1 + H_3 E_1 I_1 - [S_4^0] E_1 I_1,$$

$$J_3 = H_1 E_2 I_2 + H_1 E_1 I_3 + H_3 E_2 I_1 + H_3 E_1 I_2 + H_2 I_2 - H_4 E_1 I_1 - H_4 E_2 I_2 - [S_4^0] E_2 I_1 - [S_4^0] E_1 I_2,$$

$$J_4 = H_1 E_2 I_3 + H_2 I_3 + H_3 E_2 I_2 + H_3 E_1 I_3 - 2H_4 E_2 I_1 - [S_4^0] E_2 I_2 - [S_4^0] E_1 I_3,$$

$$J_5 = H_3 E_2 I_3 - [S_4^0] E_2 I_3,$$

$$E_1 = k_{15}/(k_{16} + k_{17}[S_{20}^*]),$$

$$E_2 = 1 + k_{12}S_3/(k_{13} + k_{14}[S_{20}^*]),$$

$$E_3 = k_{30}k_5/(k_6k_{29}),$$

$$I_1 = F_1E_1,$$

$$F_1 = k_{22}E_3 + k_4k_{21}[S_{14}^*]/(k_3[S_3^*]),$$

$$I_2 = F_1E_2 + F_2 + H_4F_1/[S_6^0],$$

$$F_2 = k_{17}[S_{12}^0][S_{20}^*]E_1 + k_{17}k_{21}[S_{14}^*][S_{20}^*][S_{12}^0]E_1/(k_3[S_3^*]),$$

$$I_3 = H_4E_2/[S_6^0].$$

$$G_1 = k_4/(k_3[S_3^*]) + 1 - E_3,$$

$$G_2 = (k_{17}[S_{20}^*] + k_3[S_3^*])[S_{12}^0]E_1/(k_3[S_3^*]),$$

$$G_3 = [S_6^0] - E_3k_6/k_5,$$

$$H_1 = G_1 + F_1/k_{22},$$

$$H_2 = G_2 + F_2/k_{22},$$

$$H_3 = G_3 + E_3k_6/k_5,$$

$$H_4 = k_{22}k_6[S_6^0]E_3/k_5,$$

References

- Kohn KW, Riss J, Aprelikova O, Weinstein JN, Pommier Y, et al. (2004) Properties of switch-like bioregulatory networks studied by simulation of the hypoxia response control system. *Mol Biol Cell* 15: 3042.
- Shen C, Powell-Coffman JA (2003) Genetic analysis of hypoxia signaling and response in *C. elegans*. *Ann NY Acad Sci* 995: 191.
- Bluthgen N, Herzel H (2003) How robust are switches in intracellular signaling cascades? *J Theor Biol* 225: 293.
- Hofer T, Desbaillets I, Hopfl G, Wenger RH, Gassmann M (2002) Characterization of HIF-1 α overexpressing hela cells and implications for gene therapy. *Comp Biochem Physiol C Toxicol Pharmacol* 133: 475.
- Kallio PJ, Wilson WJ, O'Brien S, Makino Y, Poellinger L (1999) Regulation of the hypoxia-inducible transcription factor 1 α by the ubiquitin-proteasome pathway. *J Biol Chem* 274: 6519.
- Jewell UR, Kvietikova I, Scheid A, Wenger CBRH, Gassmann M (2001) Induction of HIF-1 α in response to hypoxia is instantaneous. *FASEB J* 15: 1312.
- Kaelin W (2005) ROS: Really involved in oxygen sensing. *Cell Metabolism* 1: 357.
- Brunelle JK, Bell EL, Quesada NM, Vercauteren K, Tiranti V, et al. (2005) Oxygen sensing requires mitochondrial ROS but not oxidative phosphorylation. *Cell Metabolism* 1: 409.
- Guzy RD, Hoyos B, Robin E, Chen H, Liu L, et al. (2005) Mitochondrial complex III is required for hypoxia-induced ROS production and cellular oxygen sensing. *Cell Metabolism* 1: 401.
- Mansfield KD, Guzy RD, Pan Y, Young RM, Cash TP, et al. (2005) Mitochondrial dysfunction resulting from loss of cytochrome c impairs cellular oxygen sensing and hypoxic HIF activation. *Cell Metabolism* 1: 393.
- Jiang BH, Semenza GL, Bauer C, Marti HH (1996) Hypoxia-inducible factor 1 levels vary exponentially over a physiologically relevant range of O₂ tension. *Am J Physiol (Cell Physiol)* 40: C1172–C1180.
- Semenza GL, Wang GL (1992) A nuclear factor induced by hypoxia via de novo protein synthesis binds to the human erythropoietin gene enhancer at a site required for transcriptional activation. *Mol Cell Biol* 12: 5447–5454.
- Fall C, Marland E, Wagner J, Tyson J, editors (2005) *Computational cell biology*. New York: Springer.
- Schilling C, Letscher D, Palsson B (2000) Theory for the systemic definition of metabolic pathways and their use in interpreting metabolic function from a pathway-oriented perspective. *J Theor Biol* 203: 229.
- Wiback SJ, Palsson BO (2002) Extreme pathway analysis of human red blood cell metabolism. *Biophys J* 83: 808–818.
- Gianchandani EP, Papin JA, Price ND, Joyce AR, Palsson BO (2006) Matrix formalism to describe functional states of transcriptional regulatory systems. *PLoS Comput Biol* 2: 0902.
- Schilling C, Palsson B (1998) The underlying pathway structure of biochemical reaction networks. *Proc Natl Acad Sci U S A* 95: 4193.
- Papin JA, Stelling J, Price ND, Klamt S, Schuster S, et al. (2004) Comparison of network-based pathway analysis methods. *Trends Biotechnol* 22: 400.
- Edwards JS, Covert M, Palsson B (2002) Metabolic modelling of microbes: The flux-balance approach. *Environmental Microbiology* 4: 133.
- Bell SL, Palsson B (2004) expa: A program for calculating extreme pathways in biochemical reaction networks. *Bioinformatics* 21: 1739–1740.
- Klamt S, Stelling J, Ginkel M, Gilles ED (2003) Fluxanalyzer: Exploring structure, pathways, and flux distributions in metabolic networks on interactive flux maps. *Bioinformatics* 19: 261.
- Klamt S, Saez-Rodriguez J, Lindquist JA, Simeoni L, Gilles ED (2006) A methodology for the structural and functional analysis of signaling and regulatory networks. *BMC Bioinformatics* 7: 56.
- Raman K, Rajagopalan P, Chandra N (2005) Flux balance analysis of mycolic acid pathway: Targets for anti-tubercular drugs. *PLoS Comput Biol* 1: e46.
- Edwards JS, Palsson B (2000) The *Escherichia coli* mg1655 in silico metabolic genotype: Its definition, characteristics, and capabilities. *Proc Natl Acad Sci U S A* 97: 5528.
- Alvarez-Vasquez F, Sims K, Cowart L, Okamoto Y, Voit E, et al. (2005) Simulation and validation of modelled sphingolipid metabolism in *Saccharomyces cerevisiae*. *Nature* 433: 425.
- Edwards JS, Ibarra R, Palsson B (2001) In silico predictions of *Escherichia coli* metabolic capabilities are consistent with experimental data. *Nat Biotechnol* 19: 125.
- DC LaPorte KW, Koshland DE (1984) The branch point effect. *J Biol Chem* 259: 14086.
- Rockafellar RT (1970) *Convex analysis*. Princeton: Princeton University Press.
- Schuster S, Dandekar T, Fell D (1999) Detection of elementary flux modes in biochemical networks: A promising tool for pathway analysis and metabolic engineering. *Trends Biotechnol* 17: 53.
- El-Samad H, Kurata H, Doyle JC, Gross CA, Khammash M (2005) Surviving heat shock: Control strategies for robustness and performance. *Proc Natl Acad Sci U S A* 102: 2736.
- Goldbeter A, Koshland DE (1981) An amplified sensitivity arising from covalent modification in biological systems. *Proc Natl Acad Sci U S A* 78: 6840.
- Simon MC (2006) Coming up for air: HIF-1 and mitochondrial oxygen consumption. *Cell Metabolism* 3: 150.
- Kim J, Tchernyshyov I, Semenza GL, Dang CV (2006) HIF-1-mediated expression of pyruvate dehydrogenase kinase: A metabolic switch required for cellular adaptation to hypoxia. *Cell Metabolism* 3: 177.
- Papandreou I, Cairns RA, Fontana L, Lim AL, Denko NC (2006) HIF-1 mediates adaptation to hypoxia by actively downregulating mitochondrial oxygen consumption. *Cell Metabolism* 3: 187.

Supporting Information

Accession Numbers

Protein accession numbers as listed in Table 1 are from <http://www.ncbi.nlm.nih.gov/entrez/query.fcgi?DB=protein>.

Acknowledgments

Author contributions. YY, GW, RS, WP, FT, and CZ conceived and designed the experiments. YY and GW performed the experiments and analyzed the data. YY, GW, RS, WP, and CZ wrote the paper.

Funding. We acknowledge support from US National Science Foundation grant DMR-0313129 (CZ) and the George Washington University REF fund (CZ, FT, and RS) for this study.

Competing interests. The authors have declared that no competing interests exist.